Mon. Not. R. Astron. Soc. **000**, 000–000 (0000) Printed 26 May 2015 (MN LATEX style file v2.2)

# Galaxy Formation with Local Photoionization Feedback - II. Effect of X-Ray Emission from Binaries and Hot Gas

R. Kannan[1⋆], M. Vogelsberger[1], G. S. Stinson[2], J. F. Hennawi[2], F. Marinacci[1], V. Springel[3,4], A. V. Macciò[2]

[1] *Department of Physics, Kavli Institute for Astrophysics & Space Research, Massachusetts Institute of Technology, Cambridge 02139, MA, USA*
[2] *Max-Planck-Institut für Astronomie, Königstuhl 17, 69117, Heidelberg, Germany*
[3] *Heidelberg Institute for Theoretical Studies, Schloss-Wolfsbrunnenweg 35, D-69118 Heidelberg, Germany*
[4] *Zentrum für Astronomie der Universität Heidelberg, ARI, Mönchhofstr. 12-14, D-69120 Heidelberg, Germany*



26 May 2015

## ABSTRACT

We study how X-rays from stellar binary systems and the hot intracluster medium (ICM) affect the radiative cooling rates of gas in galaxies. Our study uses a novel implementation of gas cooling in the moving-mesh hydrodynamics code AREPO. X-rays from stellar binaries do not affect cooling at all as their emission spectrum is too hard to effectively couple with galactic gas. In contrast, X-rays from the ICM couple well with gas in the temperature range $10^4 - 10^6$ K. Idealised simulations show that the hot halo radiation field has minimal impact on the dynamics of cooling flows in clusters because of the high virial temperature ($\gtrsim 10^7$K), making the interaction between the gas and incident photons very ineffective. Satellite galaxies in cluster environments, on the other hand, experience a high radiation flux due to the emission from the host halo. Low mass satellites ($\lesssim 10^{12}$M$_\odot$) in particular have virial temperatures that are exactly in the regime where the effect of the radiation field is maximal. Idealised simulations of satellite galaxies including only the effect of host halo radiation (no ram pressure stripping or tidal effects) fields show a drastic reduction in the amount of cool gas formed ($\sim 40\%$) on a short timescale of about 0.5 Gyrs. A galaxy merger simulation including all the other environmental quenching mechanisms, shows about 20% reduction in the stellar mass of the satellite and about $\sim 30\%$ reduction in star formation rate after 1 Gyr due to the host hot halo radiation field. These results indicate that the hot halo radiation fields potentially play an important role in quenching galaxies in cluster environments.

**Key words:** atomic processes – hydrodynamics – plasmas – radiative transfer – galaxies: formation – methods: numerical

## 1 INTRODUCTION

The basic model of galaxy formation assumes that as dark matter hierarchically collapses, gas flows into gravitational potential wells and forms stars at their centers (White & Rees 1978). The gas converts gravitational potential energy into thermal energy and consequently, the gas in the halo heats up to the virial temperature, $T_{vir}$. In the most massive galaxies, the temperature becomes so large that the cooling time for the gas is longer than the age of the Universe (Rees & Ostriker 1977). In this idealised picture, gas in massive galaxies cannot cool to form stars. However, galaxy haloes have high density material in their centers, and since gas cooling is strongly dependent on density, $\Lambda \propto n^2$, this dense central gas unstably overcools and collapses to the halo center where it forms many more stars than are observed (Cole 1991; Navarro et al. 1995; Benson et al. 2003).

To counteract this overcooling, galaxy formation models feed energy back from stars (e.g.. Navarro et al. 1996; Springel & Hernquist 2003; Stinson et al. 2006; Dalla Vecchia & Schaye 2008; Vogelsberger et al. 2013; Hopkins et al. 2014) and active galactic nuclei (AGN) (e.g., Springel et al. 2005; Di Matteo et al. 2005; Sijacki et al. 2007, 2009; Booth & Schaye 2009). Stars deposit large amounts of energy through stellar winds, supernovae explosions, and radiation (Leitherer et al. 1999). Although feedback from stars is able to

⋆ Email: kannanr@mit.edu

regulate the star formation rate in low mass galaxies, they are inefficient at high masses (Kannan et al. 2014a). AGN feedback has been invoked to solve the problem in high mass haloes ($M_{halo} \gtrsim 10^{12} M_\star$).The details of how AGN couple to the gas in and around galaxies is still uncertain, so modeling efforts have so far been necessarily crude.

Springel et al. (2005), for example, used the energy from the high accretion periods of AGN when they shine as quasi-stellar objects (QSOs, quasars) to heat gas immediately surrounding the black hole and drive large scale winds. However, this level of accretion requires that a lot of cold gas is present at the center of the galaxy, which in turn leads to star formation. Even when AGNs are accreting a small amount of gas, they drive spectacular radio jets that are well collimated by magnetic fields and produce radio lobes tens of kpc away from the black holes. Cosmological numerical simulations have cited these jets as a form of feedback that is able to heat the entire gas halo to high enough temperatures that prevents gas from cooling into the disk and forming stars (Sijacki et al. 2007). However, these models do not address one of the primary features of radio mode feedback, the strong directionality of the jet. So neither of these models sufficiently explain how galaxies are quenched by AGN feedback.

Thermal conduction is another mechanism which has been invoked to stabilise the gas in clusters (Zakamska & Narayan 2003; Voit et al. 2008, 2014; Voit 2011; Voit & Donahue 2015). The large Chandra study of ICM entropy profiles (ACCEPT), showed that strong AGN feedback is present only in clusters with low-entropy cores (Cavagnolo et al. 2008, 2009). Voit et al. (2014) have postulated that the low entropy clusters have cooling times about the order of precipitation times of the clusters, which is empirically seen to occur when $t_{cool} \approx 10 t_{ff}$ (Gaspari et al. 2011, 2012). The clusters with large entropy at their centers were shown to lie above the thermal conduction balance solution, meaning that the cooling in the centers of these clusters is balanced by thermal conduction heating by hot gas at larger radii. One of the most important assumptions in this study is the value of the conduction coefficient which is about 30% the canonical Spitzer conductivity (Spitzer 1962). Thermal conductivity can reach this high value only if the magnetic field is chaotic over a wide range of length scales (factor of 100 or more), as might happen with MHD turbulence (Narayan & Medvedev 2001). However, recent studies have shown that the reproduction of observed sharp features in the ICM (cold filaments, bubbles) require that the conduction coefficient be as low as $10^{-2} - 10^{-3}$ times the Spitzer conductivity (Gaspari & Churazov 2013; Arth et al. 2014).

Cantalupo (2010) explored analytically the effect of X-ray radiation from hot shock heated gas due to stellar winds and supernovae (SNe) explosions on the cooling of halo gas. The high-energy radiation from these sources was shown to ionize metals and decrease the cooling rate of high-metallicity gas considerably. Kannan et al. (2014b, hereafter RK14b) implemented this effect using GASOLINE (Wadsley et al. 2004) and showed that in a cosmological simulation of a Milky-Way galaxy the local radiation fields indeed reduce gas cooling rate onto the disc of the galaxy thereby reducing the star formation. This formalism will not quench galaxies because of the need to form stars in order to reduce star formation. The radiation sources which can quench galaxies need to be independent of the star formation in galaxies. Either the stellar emission sources must have a time delay between the star formation event and emission or they must be of a non-stellar origin.

Gnedin & Hollon (2012) created a general model for cooling in the presence of a radiation field near a galaxy (including both stars and AGNs). They showed that these radiation fields will significantly alter the cooling rates of gas in the vicinity of a massive 'O' star and in galaxies containing highly luminous quasars. Along these lines Vogelsberger et al. (2013) introduced a AGN feedback mechanism, which modified the cooling of gas according to the incident radiation field of the central AGN. In their simulations, the radiative feedback is only effective during times when the AGN is strongly accreting and shining brightly as a quasar, which again corresponds to times when stars are forming. In the end, the only feedback that they found effective at maintaining quiescent galaxies was the AGN radio-mode feedback that operates by heating the halo gas to temperatures where its cooling time is too long to cool into the disk to form stars.

Another avenue through which galaxies can quench is through environmental effects such as ram pressure stripping (Gunn & Gott 1972; McCarthy et al. 2008; Font et al. 2008; Kang & van den Bosch 2008; Weinmann et al. 2010) and tidal stripping (Taylor & Babul 2001; D'Onghia et al. 2010; Chang et al. 2013). These quenching mechanisms are invoked to explain the different statistical properties of field and cluster galaxies, such as the prevalence of ellipticals and lower star formation rates and hence redder colors. In many prescriptions for ram pressure stripping the hot gas in the halo is assumed to be stripped immediately after the satellite falls into the host, which leads to a rapid decline in star formation rates (Baldry et al. 2006; Weinmann et al. 2006; Wang et al. 2007). More improved methods of stripping have been looked at, such as the a more gradual stripping of the hot gas reservoir (Font et al. 2008; Kang & van den Bosch 2008; Weinmann et al. 2010; McCarthy et al. 2008). However, even this formalism does not agree well with the observational measurements and they generally overproduce the quenched fraction of satellites as a function of distance from the cluster and underproduce the fraction of elliptical galaxies in cluster environments (Guo et al. 2011; Weinmann et al. 2011).

In this paper we explore the possibility that local X-ray radiation from X-ray binaries (XRBs) and bremsstrahlung cooling radiation from hot gas present in the haloes of galaxies can help to regulate star formation in galaxies. XRBs are known to be the most prominent X-ray sources in a galaxy which is devoid of an accreting black hole or large amounts of hot optically thin gas (Fabbiano & White 2003). Clusters of galaxies are the brightest extended X-ray sources in the Universe, with their luminosities ranging from $10^{44-47}$ erg $s^{-1}$ (Vikhlinin et al. 2009; Pratt et al. 2009; Anderson et al. 2014). We build on the RK14b model and account for these additional X-ray radiation fields while calculating gas cooling rates in galaxy formation simulations.

The paper is structured as follows. Section 2 describes the photoionization sources that we consider in this work. Section 3 outlines the approximations used in our radiative transfer approach, while Section 4 describes the construction of the cooling table. Finally, in Section 5 and 6, we present the results of our implementation of the local photoioniza-

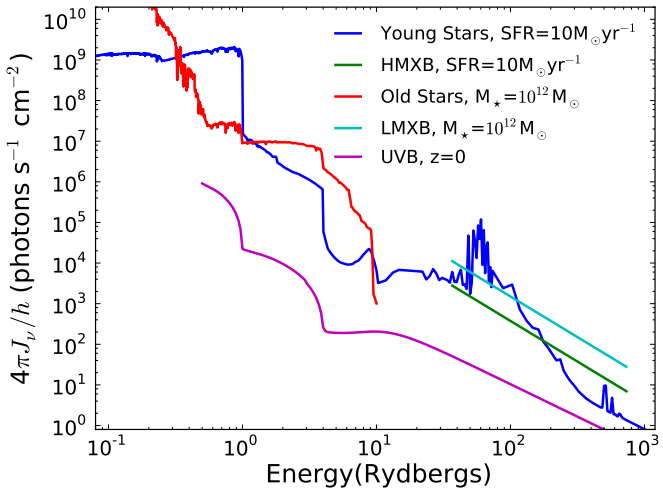


**Figure 1.** The incident photon flux as a function of energy, from high (green curve) and low (cyan curve) mass X-ray binaries compared to the radiation field from star formation events or young stars (blue curve) and from old or post-AGB stars (red curve). These fluxes are reported at 10 kpc from the source. The radiation flux from both the HMXBs and the young stars are quoted for a star formation rate of 10 $M_\odot$ yr$^{-1}$. The radiation flux from both old stars and LMXBs are quoted for a stellar mass of $M_\star = 10^{12} M_\odot$. For comparison, the estimate for the flux of the extragalactic UV background at $z = 0$ is also plotted (purple curve).

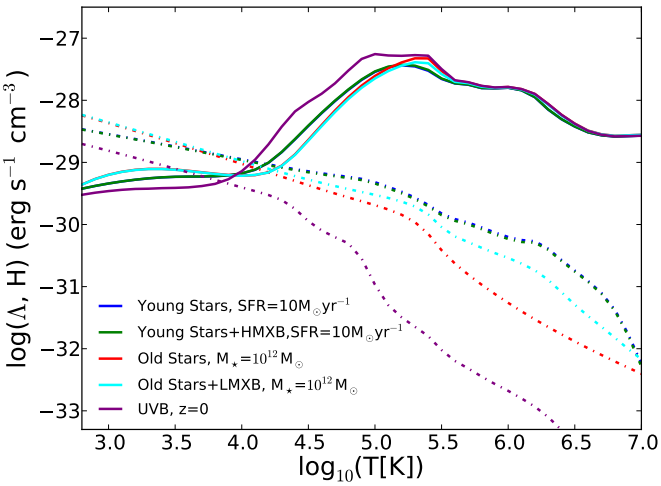


**Figure 2.** The volumetric cooling (solid curves) and heating (dot dashed curves) rates of gas under the influence of radiation from young stars and HMXBs (blue curves), only young stars (green curves), old stars and LMXBs (cyan curves), only old stars (red curves) and the extragalactic UV background (purple curves). The gas is at a density of $n_H = 0.001\text{cm}^{-3}$, and a metallicity of $Z_\odot$. The radiation flux for each component is equal to the value quoted in Fig. 1.

tion feedback (LPF) model on a test gas particle and on isolated galaxy simulations. Our conclusions are presented in Section 7.

## 2 IONIZING SOURCES

There are several radiation sources that produce high energy ionizing photons. RK14b modelled the effect of radiation from star formation events (or young stars) and post-AGB (old stars) stars. In this paper we explore the emission from X-ray binaries (XRBs) and the cooling radiation from the hot tenuous gas around haloes. Throughout this work, the estimate for the extragalactic UV background by Faucher-Giguère et al. (2009) is used.

### 2.1 X-Ray Binaries

About a third of all stars form as part of a binary system (Lada 2006). The evolutionary timescales of stars comprising the binary system may be different, leading to the collapse of one star earlier than the other. The collapsed star then acts as an accretor of material from the donor main sequence star, once the surface of the donor star crosses the inner Lagrange point of the system (Paczyński 1971). This infalling material dissipates gravitational potential energy in the form of radiation. They are the most prominent X-ray sources in galaxies which are devoid of an accreting black hole or large amounts of hot optically thin gas (Fabbiano & White 2003). The XRB population is divided into three categories depending on the mass of the donor star: high mass XRBs ($M_\star \geqslant 8\ M_\odot$), intermediate mass XRBs ($1\ M_\odot < M_\star < 8\ M_\odot$) and low mass XRBs ($M_\star \leqslant 1\ M_\odot$). The X-ray emission is dominated by high mass XRBs immediately after a star formation event, followed by a possible contribution from the intermediate mass XRB population, and the late time emission is dominated by low mass XRBs. The emission from and properties of, intermediate mass XRBs is not well studied because there are very few XRBs in this mass range in the Milky-Way galaxy (Podsiadlowski et al. 2002; Pfahl et al. 2003). Therefore, in this work we only consider the emission from the high and low mass XRB populations only.

#### *2.1.1 High Mass X-ray Binaries*

High mass XRBs (HMXBs) are binaries where the mass of the donor star is $\gtrsim 8M_\odot$. Their lifetimes are determined by the nuclear timescale of the high mass donor star, which is $1-10$ Myr. Thus, HMXB emission occurs a few million years after star formation events and the total emission luminosity of HMXBs follows the star formation rate of the galaxy. Tight empirical relations are observed between the X-ray luminosity of the HMXBs and the star formation rate of the galaxy (Grimm et al. 2003; Persic et al. 2004). Recently Mineo et al. (2012) presented the following relation for the luminosity of the HMXBs as a function of the star formation rate

$$L^{\rm HMXB}_{0.5-8\rm keV} = 2.61 \times 10^{39} \left(\frac{SFR}{1 M_\odot \rm yr^{-1}}\right) \rm erg\ s^{-1}. \quad (1)$$

Energies lower than 0.5 keV are difficult to observe, because they are absorbed in the interstellar medium of the host

as well as our own Milky-Way galaxy. We therefore model XRB emission in the hard X-ray regime only. In this regime (above 0.5 keV), the HMXB SED can be approximated by a power law:

$$\frac{dI}{dE} \propto E^{-2}, \tag{2}$$

where $I$ is the intensity and $E$ is the energy of the emitted photon. Using these relations we can plot the SED of HMXBs as a function of the star formation rate of the galaxy. Fig. 1 shows the HMXB emission spectra corresponding to a SFR of 10 $M_\odot$ $yr^{-1}$ (green curve). For comparison, the SED from young stars (see RK14b for details) is shown for the same SFR (blue curve). The fluxes quoted are at a distance of 10 kpc from the source.

Fig.2 shows the corresponding cooling (solid curves) and heating (dashed curves) rates in presence of various radiation sources. The gas parcel is at a density of $n_{\rm H} = 0.001{\rm cm}^{-3}$ and $Z = Z_\odot$ and at a distance 10 kpc from the source. The cooling curve is calculated under the assumption that the gas in between the source and the gas parcel is optically thin. Thus, the flux is inversely proportional to the distance squared. The heating (H) and cooling ($\Lambda$) curves of the gas in the presence of the young stars (blue curves) radiation field only lies exactly on top of the heating and cooling curves calculated in the presence of young stars + HMXB radiation field (green curves). In a star forming galaxy the emission from young stars (i.e., blackbody emission from stars and X-ray emission from shock heated gas) dominates the emission from HMXBs up to $\sim 180$ Rydbergs (Fig. 1). Above this energy, the hard X-ray photons do not couple effectively with the gas because of low interaction cross section. We conclude that HMXBs, although an important source of X-rays have a sub-dominant effect on the gas cooling rates in galaxies.

#### *2.1.2 Low Mass X-Ray Binaries*

Low Mass XRBs (LMXBs) are binaries where the mass of the donor star is $\lesssim 1 M_\odot$. The X-ray active phase of these systems are delayed by the nuclear timescale of the low mass donor star or by the orbital decay timescale. These timescales are $\sim 1 - 10$ Gyrs (Verbunt & van den Heuvel 1995). The duration of the X-ray active phase also has similar timescales (Podsiadlowski et al. 2002; Pfahl et al. 2003). This delay in X-ray active phase decouples the X-ray emission from the star formation event. Instead, the luminosity of LMXB correlates well with the total stellar mass of the galaxy (Gilfanov 2004), and the relation is given by:

$$L^{\rm LMXB}_{0.5-8{\rm keV}} = 1.00 \times 10^{40} \left(\frac{{\rm M}^{\rm tot}_\star}{10^{11}{\rm M}_\odot}\right) {\rm erg\ s}^{-1}. \tag{3}$$

The spectral shape of LMXB emission is assumed to follow the same functional form as Eq. 2. Fig. 1 shows the LMXB emission flux (cyan curve) for a galaxy with a total stellar mass of $10^{12} M_\odot$ at a distance of 10 kpc from its center. For comparison the flux from post-AGB stars (red curve), under similar conditions is also shown. The LMXBs contribution is primarily in the hard X-ray regime, while post-AGB stars shine only in the UV.

The corresponding cooling curves are plotted in Fig.2. The cooling curves for a parcel of gas under the influence of radiation from just post-AGB stars (red curve) and one with radiation from post-AGB and LMXBs (cyan curve) are indistinguishable, except for a slight suppression of cooling at $\log_{10}({\rm T[K]}) \sim 5.3$ in the presence of LMXB radiation field. This implies that XRBs in general do not have a significant impact on the cooling rates. This is due to a couple of factors, one, their emission fluxes are sub dominant compared to the radiation sources already considered in RK14b, i.e., young stars and post-AGB stars. And two, the hard X-ray photons have very low interaction cross sections. If we could in fact include the XRB emission at lower energies, then it could possibly have an impact on gas cooling rates. However, modelling this part of the emission spectra has so far proven to be quite challenging (Gilfanov & Bogdán 2010).

### 2.2 Hot Gas Emission

Early observations indicated that clusters are ubiquitous emitters in the X-ray regime, with luminosities $\sim 10^{42-45}$erg $s^{-1}$ (Giacconi et al. 1972). The X-ray emission is observed to be non time-varying and extended, with the spatial extent matching the galaxy distribution (Kellogg et al. 1972; Elvis 1976). These properties point to the fact that the X-ray emission arises from bremsstrahlung or free-free cooling of the hot ($T \approx 10^{7-8}$K) tenuous ($n_{\rm H} \approx 10^{-3}$ $cm^{-3}$) intracluster medium (ICM). The thermal free-free volumetric emissivity ($j_\nu^{ff}$) of a parcel of gas at temperature $T$ is given by

$$j_\nu^{ff} = \Lambda_\nu(T) n_e n_i, \tag{4}$$

where

$$\Lambda_\nu(T) = 6.8 \times 10^{-38} T^{-1/2} e^{-h\nu/kT} Z^2 g_{ff}, \tag{5}$$

where $g_{ff}$ is the free-free gaunt factor, $k$ is the Boltzmann constant, $Z$ is the mean ionic charge, $h$ is the Planck constant and $n_e$ and $n_i$ are the electron and ion particle densities respectively. The free-free emission SED is independent of the frequency at low energies and has an exponential cutoff at a characteristic frequency, determined by the temperature of the gas. This cutoff frequency shifts towards higher values as the temperature of the gas increases. The total flux on the other hand is a strong function of the density of the emitting gas parcel $j_\nu^{ff} \propto \rho^2$. Therefore, the temperature of the gas decides the hardness of the spectrum while its density controls the overall luminosity.

In order to study the effect of the X-rays from clusters on gas cooling rates, it is important to match their observed luminosities. The relation between the X-ray luminosity and the mass of the host halo has been extensively studied all the way from galaxy groups (Bharadwaj et al. 2014) to cluster scales (Vikhlinin et al. 2009; Pratt et al. 2009; Planck Collaboration et al. 2013; Wang et al. 2014). More recently Anderson et al. (2014) analyzed a sample of $\sim 250000$ locally brightest central galaxies selected from the Sloan Digital Sky Survey (SDSS) and stacked the X-ray emission from these haloes, as a function of the stellar mass of the central galaxy, using data from the ROSAT All-Sky Survey. They constrain the $L_x - M_\star$ relation in a wide range of central galaxy stellar masses shown in Fig. 3 (blue points). These values are quoted for hot gas emission between $0.15 - 1.0$ $R_{500}$ of the cluster.

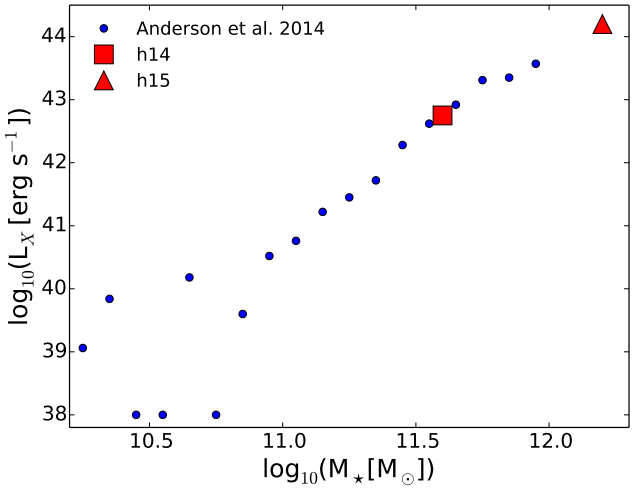


**Figure 3.** X-ray (0.5-2.0 keV) luminosities of clusters. The blue points are observational measurements taken from Anderson et al. (2014). The red square (h14) and triangle (h15) are the luminosities of the synthetic clusters calculated using Eqs. 6,7. These luminosity measurements are made between $0.15 - 1.0$ $R_{500}$.

We construct two idealised haloes containing gas and DM, one of mass ($M_{halo}$) $10^{14}$ $M_\odot$ (h14) and one of mass $10^{15}$ $M_\odot$ (h15). The DM density profile of the these haloes follows a Navarro et al. (1997) (NFW) distribution. The concentration parameter is set by the $c_{vir} - M_{halo}$ relation given in Dutton & Macciò (2014). The gas fraction of the haloes is chosen to match observations (Giodini et al. 2009; Gonzalez et al. 2013; Sanderson et al. 2013). The gas in the halo is placed in hydrostatic equilibrium with the DM and the temperature of the gas is set to the virial temperature of the halo. The properties of these haloes are shown in Table 1. These haloes are then evolved, using AREPO, with cooling, gravity and hydrodynamics turned on for 200 Myrs. The luminosities are then calculated using the following relations (see also Eq. 2 of Crain et al. 2010):

$$\begin{aligned} L_{\nu,a} &= j_{\nu,a} V_a \\ &= \Lambda_{\nu,a}(T_a) n_{e,a} n_{i,a} V_a \\ &= \Lambda_{\nu,a}(T_a) \frac{X_e}{(X_e + X_i)^2} \left(\frac{\rho_a}{\mu m_p}\right)^2 V_a \\ &= \Lambda_{\nu,a}(T_a) \frac{X_e}{(X_e + X_i)^2} \frac{\rho_a}{\mu m_p} \frac{m_a}{\mu m_p}, \end{aligned} \tag{6}$$

where $V_a$ is the volume of the $a^{th}$ gas cell, $X_e = n_e/n_H$, $X_i = n_i/n_H$, $\rho_a$ is the density of the cell, $m_p$ is the proton mass and $m_a$ is the mass the gas cell. The electron and ion densities of any given gas cell are calculated assuming a primordial composition. The total X-ray luminosity is then given by

$$L = \sum_a \int_{0.5\ \mathrm{keV}}^{2\ \mathrm{keV}} L_{\nu,a} d\nu. \tag{7}$$

The luminosity calculated using these relations for the clusters h14 (red square) and h15 (red triangle) is shown in comparison to the observational data points from Anderson et al. (2014) in Fig. 3. The stellar mass of the haloes in question are determined by the $M_\star - M_{halo}$ relation given by Kravtsov et al. (2014). The X-ray luminosity of the synthetically constructed clusters matches quite well the observationally derived values.

| Halo | $M_{halo}[M_\odot]$ | $N_{DM}$ | $N_{gas}$ | $c_{vir}$ | $\epsilon_{DM}$[kpc] | $\epsilon_{gas}$[kpc] | $f_{gas}$ |
|---|---|---|---|---|---|---|---|
| h15 | $10^{15}$ | 50000 | 100000 | 5.21 | 7.57 | 2.92 | 0.10 |
| h14 | $10^{14}$ | 50000 | 100000 | 6.56 | 3.57 | 1.27 | 0.08 |
| h511 | $5 \times 10^{11}$ | 20000 | 40000 | 8.0 | 0.82 | 0.37 | 0.15 |
| h15hr | $10^{15}$ | $2.5 \times 10^6$ | $5 \times 10^6$ | 5.21 | 1.30 | 0.60 | 0.10 |
| h212lr | $2 \times 10^{12}$ | 5000 | 10000 | 10.0 | 1.30 | 0.60 | 0.15 |

**Table 1.** Table listing the parameters of the simulated galaxies

Using the relations given by Eq. 6, we then calculate the hot gas free-free emission fluxes at 100 kpc (red curve), 300 kpc (green curve) and 1 Mpc (blue curve) from the center of the h15 cluster (shown in Fig. 4). The SEDs show the characteristic shape of free-free emission, with more than one temperature component contributing to the overall shape. At $z = 0$, the hot halo cooling flux is much larger than the contribution from the extragalactic UV background (purple curve).

The cooling curves of a gas parcel of $n_H = 0.001 cm^{-3}$ and $Z = Z_\odot$ under the influence of the h15 cluster hot-halo radiation fields are shown in Fig. 5. The reduction of cooling between $10^4$ K and $10^6$ K is quite drastic even at a distance of 1 Mpc, with Fe being the only ionic species not completely photoionized. By comparison, a gas parcel at 100 kpc is completely ionized. The only cooling contribution is from bremsstrahlung emission. The equilibrium temperature, i.e., the temperature at which the heating and cooling rates of the gas parcel are equal, under these conditions also increases to about $3 \times 10^5$ K.

Another important point to note is that the cooling rate of gas with temperatures greater than $\sim 10^{6.5}$ K does not change and seems independent of the incident radiation field. The high temperature plasma is completely thermally ionized and the only cooling mechanisms are bremsstrahlung and Compton cooling. As the virial temperature of clusters are also above $\sim 10^7$K, most of the ICM will be optically thin to the X-ray emission, which is in agreement with observations (Sarazin 1986, and references within). Therefore, the radiation field will not affect a large fraction of the cluster gas, but it will certainly reduce the cooling rate of any gas in the cluster with relatively low temperatures, either present in the form of cooling flows or as part of satellite galaxies. We can therefore conclude that the hot halo radiation fields will have a non-negligible effect on gas cooling rates in clusters.

## 3 CALCULATING THE RADIATION FIELD

In the previous section the different sources of X-ray radiation were enumerated and the hot ICM cooling radiation was shown to be important. In RK14b we used an optically thin approximation, with a fixed escape fraction for low energy photons. This allowed us to mimic absorption and at

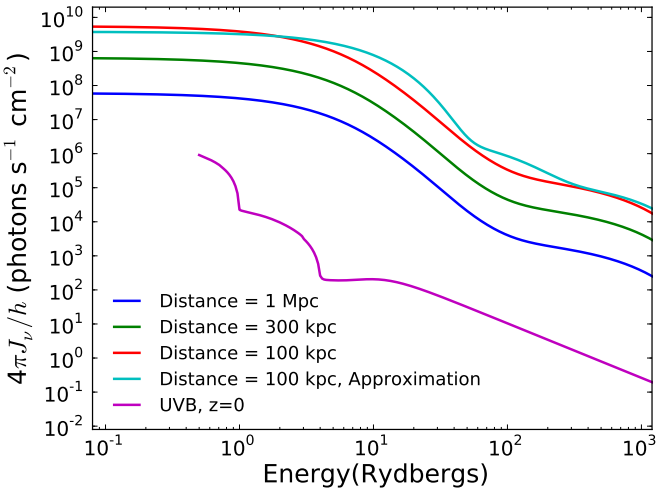


**Figure 4.** The incident photon flux as a function of energy due to bremsstrahlung emission from the hot ICM, at various distances from the center of the h15 cluster. The cyan curve is the flux at 100 kpc using the three temperature approximation described in Section 3. The other curves show the fluxes at 100 kpc (red curve), 300 kpc (green curve) and at 1 Mpc distance from the center of the cluster, calculated using the exact relations given by Eq. 6. For comparison, the estimate for the flux of the extragalactic UV background at $z = 0$ is also plotted (purple curve).

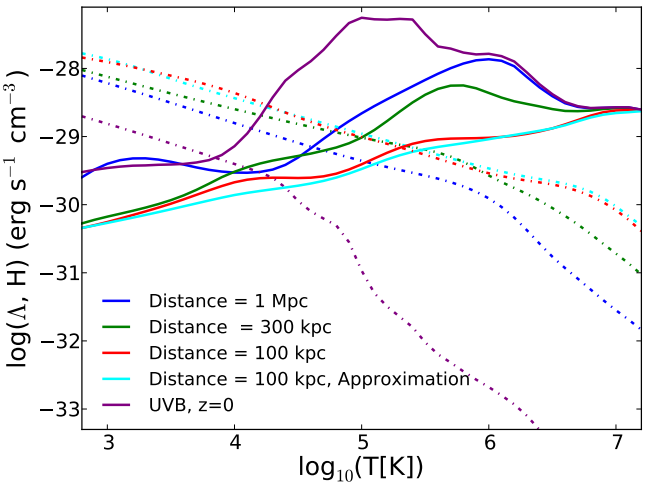


**Figure 5.** The volumetric cooling (solid curves) and heating (dot dashed curves) rates for a gas parcel under the influence of hot halo radiation field from the h15 cluster at a distance of 100 kpc (red curves), 300 kpc (green curves) and 1 Mpc (blue curves). We also show the cooling and heating rates for an SED at 100 kpc calculated using the three temperature approximation (cyan curves) described in Section 3. For comparison the cooling and heating rates in the presence of an extragalactic UV background (purple curves) at $z = 0$ is also shown. The gas is at a density of $n_H = 0.001\text{cm}^{-3}$, and a metallicity of $Z_\odot$.

the same time make the radiative transfer problem computationally feasible.

The low energy part of the XRB spectrum is not observable due to absorption by the disk of the host as well as our own Milky-Way (MW) galaxy. This necessitates that we only model XRB emission in the hard X-ray regime. The interaction cross section for the hard X-ray photons is small and hence their escape fraction from the disk of the galaxy is expected to be unity. Therefore the optically thin approximation holds for the XRB radiation fields. Additionally, we have argued in Section 2.2 that most of the hot inter cluster gas is optically thin to the radiation field. This approximation becomes invalid at the centers of the clusters, where the gas becomes dense enough to self-shield against the incident radiation field. This effect is modelled by assuming that gas above a certain density no longer sees the incident radiation field (see Section 6 for more details). Therefore the optically thin approximation is valid for both radiation fields considered in this paper making radiation transfer a simple inverse distance squared problem.

### 3.1 Three temperature approximation

The RK14b model, made a couple of simplifying assumptions in order to quantify the effect of local radiation fields on gas cooling rates in galaxy formation simulations. One, except for absorption at the source, the gas is assumed to be optically thin at all wavelengths and two, the shape of each contributing component (young stars and post-AGB stars) to the overall SED does not vary with the underlying properties of the component. For example, the model assumes that the SED from old stars is constant in shape irrespective of the age of the stellar population (as long as $t_\star \geqslant 200$ Myrs). This made sure that the spectrum of each contributing component does not change shape, rather only the overall normalisation of the spectrum varied according to the availability of and distance from the source. Therefore the photoionization ($\Gamma$) and photo heating ($\epsilon$) rates of each atomic species 'i' present in the gas, were just the sum of the individual components 'c', weighted according to their relative flux contributions '$\phi$'

$$(\Gamma_i, \epsilon_i) = \sum_c \phi_c(\Gamma_{c,i}, \epsilon_{c,i}). \quad (8)$$

This same method can be used for the XRB emission, because they scale exactly in the same way as the young stars SED (which scales with SFR) and and emission from post-AGB stars (which scales with the total stellar mass of the galaxy) considered in RK14b.

However, it is more difficult to model the emission from the hot gas. As discussed in Section 2.2, the temperature of the emitting gas parcel controls the hardness of the spectra while the density controls the overall flux. The emitted spectra of a cluster will vary depending on the gas temperature and density distribution within the cluster. Therefore, in addition to the overall normalisation, the shape of the SED also changes. The hot halo emission, therefore, cannot be quantified as one of the components of Eq. 8, instead one would theoretically need an infinite number of components, spanning the entire temperature range of the ICM. Every component of the hot halo radiation field will contribute an additional dimension to the cooling table.

Observationally, the most dominant sources of hot gas emission are galaxy groups and clusters. In lower mass haloes

the hot halo emission is orders of magnitude lower and subdominant with respect to other X-ray sources like XRBs (Bogdán et al. 2013a,b; Anderson et al. 2014; Bogdan et al. 2015). Since galaxy groups/clusters usually have virial temperatures $T > 10^{6.5}$K, we consider only cooling radiation from relatively hot gas; i.e. gas with $\log_{10}(\mathrm{T[K]}) > 5.5$. We further sub divide this hot gas into three temperature regimes, $10^6$K, $10^7$K and $10^8$K, with a spread of 0.5 dex in each direction around each temperature bin. The gas particles in each bin is then assumed to have the representative temperature of that bin. The flux from hot halo emission at any point 'p' is then approximated as

$$F^{ff}_{\nu,p} = \sum_t \Lambda_\nu(10^t) \frac{X_e}{(X_e + X_i)^2} \frac{1}{4\pi} \phi_{Tt,p} \ , \ t \in [6, 7, 8], \tag{9}$$

where

$$\phi_{Tt,p} = \sum_a \frac{\rho_a m_a}{|\vec{r}_a - \vec{r}_p|^2 \mu^2 m_p^2} \quad \forall \text{ particles 'a'}, \tag{10}$$

such that

$$t - 0.5 < \log_{10}(\mathrm{T_a[K]}) \leqslant \mathrm{t} + 0.5. \tag{11}$$

This approximation reduces the number of components of the hot halo emission radiation to three. The SED of each component has a fixed shape due to the fixed temperature and the normalisation just depends on the density times the mass of the particles within that temperature range. To check the validity of this approximation we plot, in Fig. 4, the radiation flux at a point 100 kpc from the center of the h15 cluster using the approximation (cyan curve) compared to the flux at the same point using exact relations (red curve) described in Section 2.2. The approximated SED matches quite well with the actual SED, with slight differences especially in the regime where the SED changes shape, around 100 Rydbergs. The corresponding cooling curve is plotted in Fig. 5. The heating rates (dot dashed lines) lie on top of each other, while there seems to be a small difference to the cooling component. This difference is however of the order of $0.05 - 0.1$ dex. Compared to the computational simplicity it offers, the errors induced by the approximation are quite small.

### 3.2 Propagating the radiation field

Now that we have found an effective way to quantify XRBs and hot halo emission, we need to come up with a computationally efficient method to propagate the radiation field over the whole simulation volume. We have argued that the radiation fields considered in this work, for all practical purposes, can be assumed to be optically thin. This allows us to quantify the flux from each component in the parameter '$\phi$', which is proportional to the availability of the sources and inversely proportional to square of the distance between the source and the sink.

We use the same method described in RK14b to calculate the flux of the radiation field; i.e. we tag on to the gravity tree of the simulation code. The tree structure partitions the mass distribution into a hierarchy of localised regions. The force from nearby particles is calculated accurately, while the distant regions are explored more coarsely by treating them as single massive pseudo-particles, centered on the center of mass of the corresponding region. In RK14b we implemented the LPF model in GASOLINE (Wadsley et al. 2004) which used a k-D (binary) tree structure (Stadel 2001) in which bisections are done recursively through their longest axis of the cells, whereas, in this paper we implement the model in AREPO (Springel 2010) which uses the same oct-tree (Barnes & Hut 1986) structure as GADGET-2 (Springel et al. 2005). Although these codes differ in the actual construction of the gravity tree, they are the same for our purposes.

One very simple improvement we have made, while tagging on to the gravity tree in AREPO is to consider an effective center mass of the node while calculating the distance between the node and the sink position. The effective center of mass of a radiation field component 'c' in any node is defined as the center of effective mass of all the particles in that node that contribute to that particular component. The effective mass of a component in turn is defined as quantity that controls the normalisation of the SED of that component. For example, effective mass of the new stars SED component is just the mass of stars less than 10 Myr old (see RK14b for more details), while the effective mass of the hot halo emission components is the the mass times the density of the gas particles. This assures that the effective center of mass of a component in the node is close to the point in the node where the contribution to that particular component is maximum.

## 4 COOLING TABLE CREATION

We tabulate the gas cooling rates under various gas densities, temperatures and incident radiation fields. The total gas cooling rate is divided into primordial, metal and Compton cooling (Eq. 15 of RK14b). The primordial and Compton cooling rates are calculated on-the-fly (see Vogelsberger et al. 2013 for more details). The metals are assumed to be in ionization equilibrium and their heating and cooling rates are tabulated across a range of physical conditions using CLOUDY. This look-up table is then used in simulations.

Above $z = 9$, the gas is assumed to be of purely primordial composition, negating the need for a metal cooling table. From $z = 9$ to $z = 3$ the cooling table has five dimensions corresponding to the temperature, density, flux from new stars ($\mathrm{t}_\star \leqslant 10$ Myrs), flux from old stars ($\mathrm{t}_\star \geqslant 200$ Myrs) and redshift components. At $z < 3$ the table has eight dimensions, the additional dimensions corresponding to the three hot halo emission components, which start to become dominant only at low redshifts once sufficiently massive haloes start forming.

The density ranges from $10^{-9}$ to $10^4$ cm$^{-3}$ with a spacing of 1.0 dex in log space. The temperature ranges from $10^2$ to $10^9$ K with a resolution of 0.1 dex. $\phi_{SFR}$, which quantifies radiation from young stars and the HMXBs, varies from $10^{-5}$ to $10^3$ M$_\odot$ yr$^{-1}$ kpc$^{-2}$. $\phi_{os}$, which quantifies the radiation field from post-AGB stars and LMXBs, varies from $10^6$ to $10^{12}$ M$_\odot$ kpc$^{-2}$. The spacing for both these $\phi$'s is 1.0 dex. All three hot halo components, $\phi_{\mathrm{T6}}$, $\phi_{\mathrm{T7}}$ & $\phi_{\mathrm{T8}}$, ranges from $10^{17.5}$ to $10^{23.5}$ cm$^{-5}$, with a spacing of 2.0 dex. The redshift dimension that accounts for the change in UV background ranges from 0.0 to 9.0 with a resolution of 0.5.

To create the table, cooling and heating rates are cal-

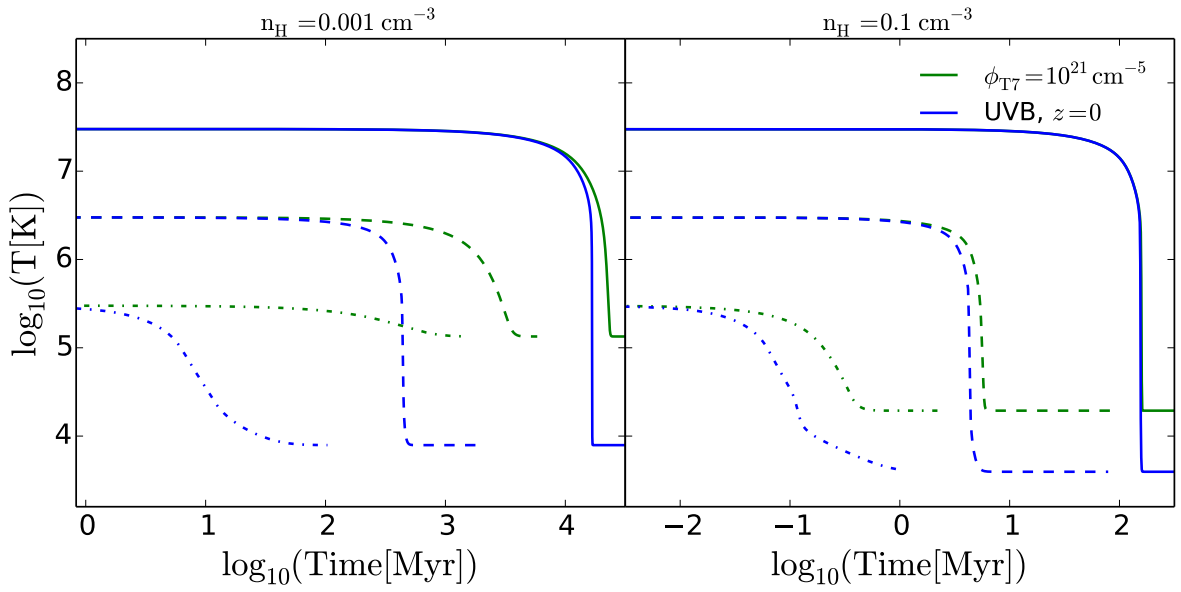


**Figure 6.** The temperature evolution of gas parcels with densities $n_H = 0.001$ cm$^{-3}$ (left panel) and $n_H = 0.1$ cm$^{-3}$ (right panel) and temperatures $3 \times 10^7$K (solid curves), $3 \times 10^6$K (dashed curves) and $3 \times 10^5$K (dot dashed curves). Each gas parcel is subjected to two different radiation fields, one which contains hot halo radiation field of strength $\phi_{T7} = 10^{21}$ cm$^{-5}$ plus the extragalactic UV background at $z = 0$ (green curves) and other which contains only the extragalactic UV background flux at $z = 0$ (blue curves).

culated at every point of phase space for solar and primordial metallicity gas using CLOUDY. The difference between the solar and primordial metallicity values are stored as the heating and cooling rates due to metals only.

## 5 TEST PARTICLE EVOLUTION

As a first test of the cooling implementation in AREPO, we calculate the temperature evolution of isolated gas cells with and without hot halo radiation fields (Fig. 6). We consider gas cells of density of $n_H = 0.001$ cm$^{-3}$ (left panel) and $n_H = 0.1$ cm$^{-3}$ (right panel), metallicity $Z = Z_\odot$ and starting temperatures $3 \times 10^7$K (solid curves), $3 \times 10^6$K (dot dashed curves) and $3 \times 10^5$K (dot dashed curves). The temperature evolution of these six gas cells under the the influence of a hot halo radiation field of strength $\phi_{T7} = 10^{21}$ cm$^{-5}$ plus the UV background at $z = 0$ (green curves) and under the influence of a UV background radiation field at $z = 0$ only (blue lines) are shown.

The effect of the radiation field on the cooling rates of the gas cells is highly dependent on both the starting temperature and density of the cell. At a particular density, the initial temperature of the gas decides the effectiveness of the radiation fields. The temperature evolution of the $3 \times 10^7$ K gas cell (at both densities) is barely effected. The time it takes for this high temperature gas cell to cool from $3 \times 10^7$K to $10^6$K is much longer ($\sim 20$ Gyrs for $n_H = 0.001$ cm$^{-3}$) than to cool from $10^6$K to the equilibrium temperature ($\sim 1.7$ Gyrs for $n_H = 0.001$ cm$^{-3}$). Therefore, even if the radiation fields drastically increases the cooling time from $10^6$K to $10^4$K (as seen in Section 2.2), the total cooling time will not change by a lot.

Another notable change between the temperature evolution of gas cells with and without the hot halo radiation fields is the increase in the minimum temperature for each particle from $\sim 10^4$K to $\sim 10^5$K. The minimum temperature reflects the equilibrium temperature the radiation field sets. While $10^5$ K is a higher temperature than that at which stars form, it is not high enough to support against collapse with thermal pressure in cluster environments. As we will see in next section, $10^5$K gas collapses into a center that eventually reaches a high enough density to cool regardless of the radiation field.

The cooling rates of the low temperature gas parcels ($3 \times 10^6$K & $3 \times 10^5$K) on the other hand are reduced quite drastically. In the presence of the hot halo radiation field the equilibration timescale is about 7 times higher for $3 \times 10^6$K gas parcel and 25 times higher for $3 \times 10^5$K gas parcel at $n_H = 0.001$ cm$^{-3}$. In galaxies with $T_{vir} < 10^{6.5}$K, the cooling and star formation timescales are inherently smaller. Therefore an increase in the cooling time of the gas particle will definitely affect the star formation rates of the galaxy. This implies that any galaxy that is close to or is falling into the cluster will experience substantial quenching, due to the host halo radiation field.

The density of the gas also plays a major role in its cooling rates. As we discussed in Section 2.2, the volumetric cooling rate is proportional to the square of the density, which in turn means that the cooling time of the gas parcel will be inversely proportional to the density of the gas ($t_{cool} = 3nk_BT/2\Lambda$). This affect can clearly be seen in Fig. 6, where the cooling times of gas cells with $n_H = 0.1$ cm$^{-3}$, irrespective of their starting temperature, is about a 100 times shorter than the cells with $n_H = 0.001$ cm$^{-3}$. This means that galaxies with higher mean gas densities will have a larger cooling flow.

Additionally the effect of the radiation fields will also

reduce at higher densities. We can define an ionization parameter (U) for the gas parcel as

$$U = \frac{4\pi}{hcn}\int_{\nu_T}^{\infty}\frac{J_\nu}{\nu}d\nu, \tag{12}$$

where $c$ is the speed of light, $h$ is the Planck constant, $n$ is the particle density and $\nu_T$ is the threshold frequency for ionization (13.6eV for hydrogen atom). This parameter is basically the ratio between the number density of ionizing photons incident on the gas cell to the number density ionic species in that cell. For a fixed radiation field the ionization parameter decreases as the density of the cell increases. A decrease in the ionization parameter, implies a decrease in the effectiveness of the incident radiation field. This effect is seen Fig. 6, where the relative difference in cooling times of the gas cells under the presence and absence of hot halo radiation fields is much smaller for the high density gas cells. For example, the gas cell with $T_{start} = 3\times10^7$K (solid curves) has a three fold increase in the cooling time due to the hot halo radiation field when it has a density of $n_H = 0.001$ cm$^{-3}$, but the cooling times are practically identical when we increase the density of the cell to $n_H = 0.1$ cm$^{-3}$. This means that galaxies with lower mean densities will be more amenable to reduction in cooling rates due to local radiation fields.

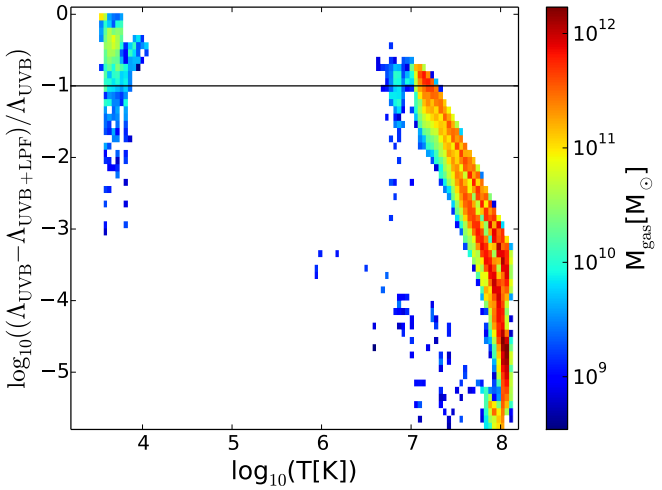


**Figure 7.** A 2-D histogram of the amount of gas mass in the h15 cluster plotted as a function of the change in cooling rate between the UVB and UVB+LPF simulation runs and temperature at the end of 0.5 Gyr of evolution.

## 6 RESULTS

In order to study the effect of the hot halo radiation fields in a full dynamical setting, we perform isolated galaxy simulations. Specifically, we simulate the idealised clusters h14 and h15 (see Section 2.2 for more details about the construction and properties of these clusters).

### 6.1 Host Halo Quenching

We simulate two clusters of halo mass $10^{14}$ M$_\odot$ (h14) and $10^{15}$ M$_\odot$ (h15). The only physical processes considered are gravity, hydrodynamics and gas cooling. A very simple prescription for self shielding is also included by imposing the condition that all gas particles with $n_H \geqslant 0.1$ cm$^{-3}$ (Ceverino et al. 2010) have zero local radiation flux. All the gas in the halo is assumed to have a metallicity of $0.3Z_\odot$, a value chosen to match the observational constraints from nearby clusters (Sato et al. 2009).

Each cluster is simulated twice, once with gas cooling rates calculated in the presence of the UV background radiation field at $z = 0$ only (UVB) and once with the hot halo radiation field turned on in addition to the UV background (UVB+LPF). The simulations are run for 0.5 Gyr. The percentage change in the amount of cold gas ($T \leqslant 10^4$K) formed between UVB and UVB+LPF simulation for the h14 and h15 clusters is rather minimal ($\lesssim 3\%$). This is because the virial temperature of clusters are high enough to fully thermally ionize the gas, which reduces the effectiveness of the incident radiation fields. This is seen more clearly in Fig. 7, which shows the amount of gas mass as a function of temperature and the change in cooling rate between the UVB and UVB+LPF simulations for the h15 cluster. Most of the gas in the halo lies in the region with $T > 10^{7.5}$K, where the change in cooling rate is pretty minimal. There is a $\gtrsim 10\%$ (denoted by the solid horizontal black line in the Fig. 7) decrease in the cooling rate of the UVB+LPF simulation only in the region where $T < 10^{7.5}$K. However, the amount of gas in this region of the plot is only a small fraction of the total gas mass. There is in fact a wide region between $10^4$K and $10^6$K, devoid of gas, because the cooling time in this region is much lower than the dynamical time of the system. Below $10^4$K the radiation field does have a large effect, but gas at this temperature will enter the modified equation of state according to the ISM model used in our simulations (Springel & Hernquist 2003), meaning that it has already been earmarked for star formation. Therefore, changing the cooling of this gas will not reduce the star formation rate in our simulations.

Another way to quantify the effect of local radiation fields is to look at the change in cooling timescales as a function of the free-fall time of the system. Voit et al. (2014) have shown that clusters with on-going star formation and/or AGN activity have cooling times about the order of precipitation time scales in clusters, which are empirically seen to occur when $t_{ff} < t_{cool} < 20t_{ff}$ (Gaspari et al. 2011, 2012), whereas, clusters with no star formation or AGN activity were shown to lie above this precipitation zone, meaning some mechanism, other than SF or AGN, is responsible for stabilising the cooling in these haloes. Fig. 8 shows the gas cooling times as a function of radii for both the h14 (blue curves) and h15 (green curves) cluster simulations. The solid lines show the cooling times for the UVB simulation and the dot-dashed lines show the cooling times for the UVB+LPF simulation. These values are shown for the cluster after 0.5 Gyr of evolution. In the h15 cluster the UVB and UVB+LPF cooling times lie on top of one another, however, the h14 cluster does show a modest increase, a factor of 2, in the cooling times in the center. There are a couple of reasons why the radiation field is marginally more effective in the h14 cluster. One, the virial temperature of the h14 cluster is lower, meaning that the photons are more likely to inter-

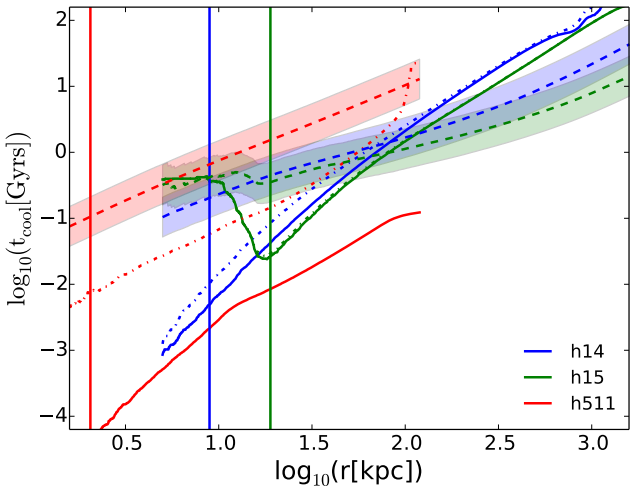


**Figure 8.** Cooling time plotted as a function of radius in the h14 (blue curves), h15 (green curves) and h511 (red curves) simulations. The dashed lines are $10t_{ff}$, and the corresponding shaded regions are $5t_{ff}$ to $20t_{ff}$. The solid lines represent the cooling rates in the UVB simulation while the dot-dashed lines are the cooling rates in the UVB+LPF simulations. The vertical lines are $r = 2.5\epsilon$ above which the properties of the galaxies are well resolved.

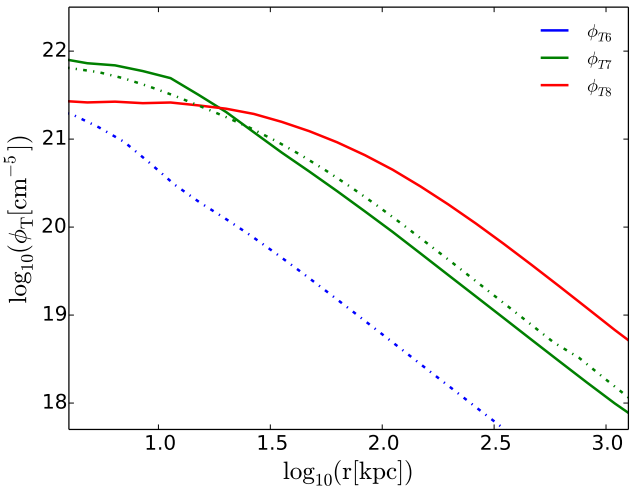


**Figure 9.** Radiation field intensity plotted as a function of radius for the h14 (dot-dashed curves) and h15 (solid curves) clusters separated into the three temperature components $\phi_{T6}$ (blue curves), $\phi_{T7}$ (green curves) & $\phi_{T8}$ (red curves).

act with the gas. Two. the free fall times in the h14 cluster are slightly longer, meaning a lower central density, which in turn decreases the density of the gas. This decreased gas density increases the cooling times and will also be more amenable to reduction in cooling rates due to local radiation fields (see Section 5). However, in neither cluster is the effect of the radiation field strong enough to increase the cooling timescales above the precipitation timescales of the system.

We find that the low density gas present in the outskirts of the cluster has too high a temperature for the radiation field to effectively couple with it. On the other hand, the relatively cold gas, with large photon interaction cross sections, are at too high a density, thereby reducing the effect of the radiation fields. We therefore conclude that hot halo radiation fields cannot significantly impact star formation in massive clusters.

### 6.2 Satellite Quenching

We have shown in Section 2.2 and Section 5, that the cooling rate of warm-hot gas ($10^4 - 10^6$K) in clusters is significantly reduced in the presence of hot halo radiation fields. It follows that in systems where the dynamical timescales are similar to the cooling time of the warm-hot gas, the effect of the radiation fields will be much more pronounced. Low mass galaxies ($M_{halo} \lesssim 10^{12} M_\odot$) have virial temperatures in the range of $10^4 - 10^6$K and the dynamical timescales of the system are of the order of $\sim 100$ Myrs. This means that a hot halo radiation field, such as the one due to the ICM of the h15 cluster, will change the dynamics of cooling flows in low mass systems. Therefore, satellite galaxies within the cluster will be adversely affected by this "radiation quenching" mechanism.

To test this scenario, we construct a galaxy of mass $5 \times 10^{11}$ $M_\odot$, labelled h511, in the same way as described in Section 2.2. The properties of this galaxy are given in Table 1. The virial temperature of this halo is $10^{5.8}$K. As shown in Section 2.2, the radiation field of the cluster varies with the distance from the center (Fig. 4). Therefore the position of the satellite within the cluster will determine how effective the host radiation fields can be. Fig. 9, shows flux in each component of the hot halo radiation field, ($\phi_{T6}$ blue curve, $\phi_{T7}$ green curve, $\phi_{T8}$ red curve), as a function of distance from the center of the corresponding cluster (h14 - dot dashed curves and h15 - solid curves). The virial temperature of the h15 cluster is $\sim 10^8$K, therefore the amount of gas in the $10^{5.5} < T \leqslant 10^{6.5}$K range is negligible and hence the $\phi_{T6}$ component is sub-dominant. Whereas, the virial temperature of the h14 cluster is $\sim 10^7$K, hence the $\phi_{T8}$ component is non-existent.

We place the h511 halo at a distance of 100 kpc (blue curves) and 300 kpc (green curves) in both the h14 (dot dashed curves) and h15 (solid curves) clusters and simulate the galaxy for 0.5 Gyrs with the host halo radiation field turned on.

There is $\sim$ 40% reduction in the amount of cool ($T < 10^4$K) gas formed (Fig. 10), if the satellite is placed at a distance of 100 kpc from the center of the h15 cluster compared to the field and the effect reduces to $\sim$ 20% at the distance of 300 kpc from the center. The effect is smaller if the galaxy is placed in the h14 halo with the reduction in amount of cool gas about 10%.

Now the question arises as to why we see an affect on low mass galaxies. To answer this we plot the gas mass of the satellite as a function of the fractional change in the cooling rate of gas between the UVB and UVB+LPF simulations and its temperature, when placed at a distance of 100 kpc from the center of the h15 cluster (Fig. 11). The cooling rates of almost all the gas in the satellite is severely reduced in the presence of the host radiation field. This in

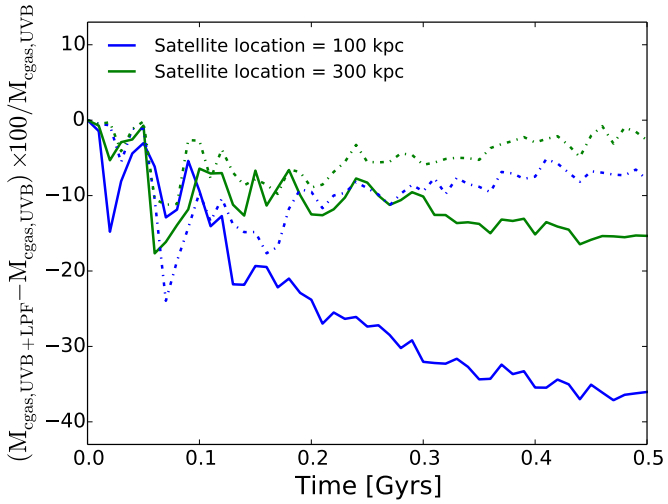


**Figure 10.** Percentage change in the amount of cold gas ($T < 10^4$K) formed between the UVB+LPF and UVB simulations as a function of time in the h511 galaxy simulation when placed at 100 kpc (blue curves) and 300 kpc (green curves) from the center of the h15 (solid curves) and h14 (dot dashed curves) clusters.

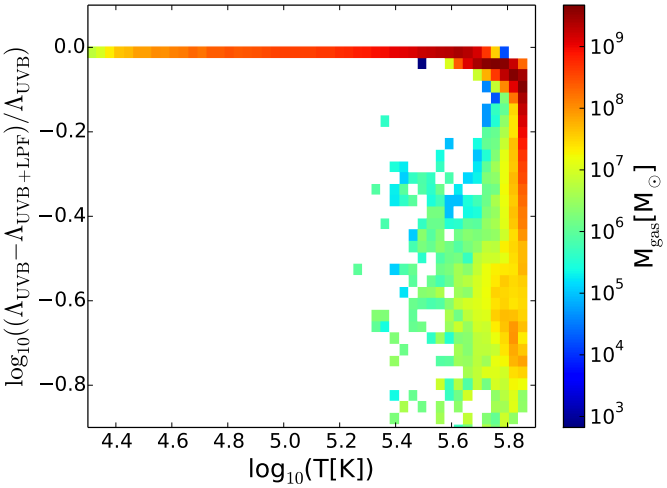


**Figure 11.** A 2-D histogram of the amount of gas mass in the h511 halo plotted as a function of the change in cooling rate between the UVB and UVB+LPF simulation runs and temperature at the end of 0.5 Gyr of evolution. The h511 galaxy is assumed to be at a distance of 100 kpc from the center of the h15 cluster.

turn causes a reduction in the amount of cooling flow and hence a reduction in the amount of cold gas formed. In contrast the amount of gas with reduced cooling rates due to the hot halo radiation field was minimal for the host cluster (see Fig. 7).

Fig. 8 shows the cooling time of the gas in h511 halo, at a distance of 100 kpc from the center of the h15 cluster, as a function of radii (red curves). In the absence of local radiation fields the cooling time scales (red, solid curve) are $\sim 10^{-4}$ $t_{prep}$ (red, dashed curve and shaded region), implying a high star formation rate. The radiation fields increase the cooling times by a factor of about $100 - 1000$ (red, dot-dashed curve), making them only a order of magnitude lower than the precipitation timescales. This huge effect is due to the fact that, unlike clusters, most of the gas in the satellite is at exactly the temperatures at which the ionization cross section in maximum ($< 10^6$K), and at low densities, as evidenced by the constantly higher free fall times in the satellite. These increased cooling times will lead to a drastic reduction in star formation rate of the galaxy, just because of lower amounts of cooling flows (see RK14b).

### *6.2.1 Relative effectiveness of the radiation quenching mechanism*

Radiation quenching complements other environmental quenching mechanisms such as ram pressure (Gunn & Gott 1972; McCarthy et al. 2008; Font et al. 2008; Kang & van den Bosch 2008; Weinmann et al. 2010) and tidal stripping (Taylor & Babul 2001). Therefore, it is important to understand the impact of radiation quenching in the presence of these other environmental quenching mechanisms. McCarthy et al. (2008) have found that for satellite galaxies with typical structural and orbital parameters, up to 30% of the initial hot halo gas can remain with the galaxy for up to 10 Gyr. During this phase it was assumed that the halo gas will continually cool and replenish the disk and sustain star formation in the satellite. However, our results show that the host halo radiation fields will reduce the star formation in these satellites to a certain extent, even before they are completely stripped of gas.

To test this scenario we run a non-cosmological merger simulation of a $2 \times 10^{12}$ $M_\odot$ halo falling into a $10^{15}$ $M_\odot$ cluster. We construct a high resolution version of the h15 cluster, where the DM distribution is sampled by 2.5 million particles and the gas distribution sampled by 5 million particles (h15hr). The galaxy of mass $2 \times 10^{12}$ $M_\odot$ (h212lr) is sampled with 5000 DM particles and 10000 gas cells. These galaxies are constructed in the same way as described in Section 2.2 and the properties of them are listed in Table 1. The h212lr satellite galaxy is placed at the virial radius of the h15hr cluster with the velocity of the satellite given by the relations outlined in Benson (2005). The system is then evolved for 1 Gyr with (UVB+LPF) and without (UVB) the hot halo radiation fields turned on. In addition to gravity, hydrodynamics and gas cooling, we also turn on star formation and stellar feedback according to the models described in Vogelsberger et al. (2013).

Fig. 12 shows the amount of stellar mass (solid curves) formed and the instantaneous star formation rates (dashed curves) in the h212lr galaxy as it falls in and orbits around the h15hr cluster. The amount of stellar mass formed after 1 Gyr is about 20% lower in the UVB+LPF run (red curve) compared to the UVB run (green curve). Additionally, the star formation rate in the UVB+LPF simulation is also about $20-30$% lower. These results suggest that even in the presence of other environmental quenching mechanisms, radiation quenching plays a significant role in reducing star formation and stellar mass in cluster environments. Therefore, they can in principle account for the reduced star formation rates of galaxies in cluster environments (Poggianti et al. 1999; Mei et al. 2009) and also explain why local qui-

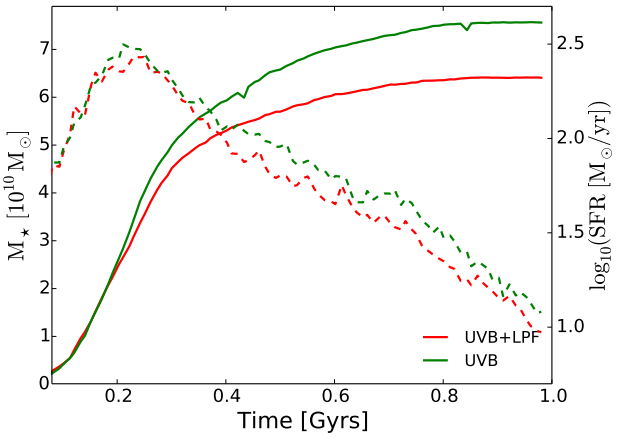


**Figure 12.** The amount of stellar mass formed (solid curves) and the instantaneous star formation rate (dashed curves) in the UVB+LPF (red curves) and UVB (green curves) runs as a function of simulation time in the h212lr satellite halo, when orbiting the h15hr cluster.

escent galaxies are observed to be quenched by a "strangulation" mechanism rather than by sudden outflows of gas due to SNe feedback or ram pressure stripping (Peng et al. 2015; Lu et al. 2015).

## 7 CONCLUSIONS

In this paper, we present first simulations of galaxy formation which include the impact X-ray emission from binaries and hot ICM on gas cooling rates using the AREPO code.

We find the observed X-ray flux from XRBs to be subdominant compared to other stellar radiation sources, minimally affecting the gas cooling rates in galaxies. However, hot gas emission from clusters has a high photon flux all the way to the virial radius of the halo. This is because the ICM is an extended source, therefore the bremsstrahlung emission from the ICM will not fall off as rapidly as radiation from centralised sources like stars. The gas cooling rates are substantially reduced, especially in the $10^4\mathrm{K} < \mathrm{T} < 10^6\mathrm{K}$ regime, under the influence of these radiation fields.

We test our model in a full dynamical setting by simulating idealised clusters of mass $10^{14}$ $\mathrm{M}_\odot$ and $10^{15}$ $\mathrm{M}_\odot$. The difference between the amount of cold gas ($\mathrm{T} < 10^4\mathrm{K}$) formed between the simulations with and without local radiation feedback is minimal, because the cooling flows are not affected by the local radiation sources in clusters. This is because the low density gas present in the outskirts of the cluster is at too high a temperature for the radiation field to effectively couple with it. On the other hand, the relatively cold gas, with large photon interaction cross sections, are at too high a density, which reduces the effectiveness of the radiation fields. This means that, even though there is enough energy in the form of radiation to quench gas cooling in clusters, the coupling between the gas and the radiation field is too weak. We conclude that the radiation fields considered in this paper will not have a major effect on star formation rates in massive galaxies.

The cooling rate of relatively cold gas ($T < 10^6\mathrm{K}$) on the other hand is reduced considerably by the hot-halo radiation field. The change in the cooling rate can be as large as the 30 times the fiducial value. This can in principal change the dynamics of cooling flows in the systems where the dynamical timescales are comparable to the cooling timescales of gas. This implies that relatively low mass satellites ($\mathrm{M_{halo}} \lesssim 10^{12}\mathrm{M}_\odot$) will experience quenching due to the radiation field of the host halo in cluster environments. We tested this idea by simulating a low mass galaxy ($\mathrm{M_{halo}} = 5 \times 10^{11}$ $\mathrm{M}_\odot$) in the presence of host halo radiation fields. We placed the satellite galaxy at a various distances from the center of the cluster and assumed that all gas in the satellite sees a host halo radiation field corresponding to that distance. These simulations show an apparent reduction in the amount of cold gas formed when the host halo radiation field is turned on. At a distance of 100 kpc from the center of the halo, the satellite has a $\sim 40\%$ reduction in cold gas mass in 0.5 Gyrs. This reduces to about 20% at 300 kpc and reduces further at larger radii. This effect is due to the fact that, unlike clusters, most of the gas in the satellite is at exactly the temperatures at which the ionization cross section is largest ($T < 10^6\mathrm{K}$), and have low enough densities, to be highly influenced by the radiation field.

We also compared the effectiveness of radiation quenching to other environmental quenching mechanisms (e.g., ram pressure stripping) by running a galaxy merger simulation of a $2{\times}10^{12}$ $\mathrm{M}_\odot$ halo falling into $10^{15}$ $\mathrm{M}_\odot$ halo. The UVB+LPF simulation shows a 20% reduction in the stellar mass of the satellite after 1 Gyr with respect to the UVB-only simulation. We also find a reduction of $\sim 20-30\%$ in star formation rates at late times. These results indicate that even in the presence of other environmental quenching mechanisms, the hot halo radiation fields still play a significant role in quenching galaxies in cluster environments.

We note that these results are preliminary and we plan to extend this initial study to a full cosmological simulation and quantify the effectiveness of the local radiation fields on satellite quenching in a wide range of satellite and host galaxy masses.

## ACKNOWLEDGEMENTS

The simulations were performed on the joined MIT-Harvard computing cluster supported by MKI and FAS and the Milky Way supercomputer, funded by the Deutsche Forschungsgemeinschaft (DFG) through Collaborative Research Center (SFB 881) 'The Milky Way System (subproject Z2), hosted and cofunded by the Jülich Supercomputing Center (JSC). We greatly appreciate the contributions of these computing allocations. GSS, VS and AVM acknowledge support from SFB 881 'The Milky Way System (subproject A1) of the German Research Foundation (DFG). JFH acknowledges generous support from the Alexander von Humboldt foundation in the context of the Sofja Kovalevskaja Award. The Humboldt foundation is funded by the German Federal Ministry for Education and Research.

**REFERENCES**


Anderson M. E., Gaspari M., White S. D. M., Wang W., Dai X., 2014, ArXiv e-prints

Arth A., Dolag K., Beck A. M., Petkova M., Lesch H., 2014, ArXiv e-prints

Baldry I. K., Balogh M. L., Bower R. G., Glazebrook K., Nichol R. C., Bamford S. P., Budavari T., 2006, MNRAS, 373, 469

Barnes J., Hut P., 1986, Nature, 324, 446

Benson A. J., 2005, MNRAS, 358, 551

Benson A. J., Bower R. G., Frenk C. S., Lacey C. G., Baugh C. M., Cole S., 2003, ApJ, 599, 38

Bharadwaj V., Reiprich T. H., Schellenberger G., Eckmiller H. J., Mittal R., Israel H., 2014, A&A, 572, A46

Bogdán Á., Forman W. R., Kraft R. P., Jones C., 2013a, ApJ, 772, 98

Bogdán Á. et al., 2013b, ApJ, 772, 97

Bogdan A. et al., 2015, ArXiv e-prints

Booth C. M., Schaye J., 2009, MNRAS, 398, 53

Cantalupo S., 2010, MNRAS, 403, L16

Cavagnolo K. W., Donahue M., Voit G. M., Sun M., 2008, ApJ, 682, 821

Cavagnolo K. W., Donahue M., Voit G. M., Sun M., 2009, ApJS, 182, 12

Ceverino D., Dekel A., Bournaud F., 2010, MNRAS, 404, 2151

Chang J., Macciò A. V., Kang X., 2013, MNRAS, 431, 3533

Cole S., 1991, ApJ, 367, 45

Crain R. A., McCarthy I. G., Frenk C. S., Theuns T., Schaye J., 2010, MNRAS, 407, 1403

Dalla Vecchia C., Schaye J., 2008, MNRAS, 387, 1431

Di Matteo T., Springel V., Hernquist L., 2005, Nature, 433, 604

D'Onghia E., Vogelsberger M., Faucher-Giguere C.-A., Hernquist L., 2010, ApJ, 725, 353

Dutton A. A., Macciò A. V., 2014, MNRAS, 441, 3359

Elvis M., 1976, MNRAS, 177, 7P

Fabbiano G., White N. E., 2003, ArXiv Astrophysics e-prints

Faucher-Giguère C.-A., Lidz A., Zaldarriaga M., Hernquist L., 2009, ApJ, 703, 1416

Font A. S. et al., 2008, MNRAS, 389, 1619

Gaspari M., Churazov E., 2013, A&A, 559, A78

Gaspari M., Melioli C., Brighenti F., D'Ercole A., 2011, MNRAS, 411, 349

Gaspari M., Ruszkowski M., Sharma P., 2012, ApJ, 746, 94

Giacconi R., Murray S., Gursky H., Kellogg E., Schreier E., Tananbaum H., 1972, ApJ, 178, 281

Gilfanov M., 2004, MNRAS, 349, 146

Gilfanov M., Bogdán Á., 2010, Nature, 463, 924

Giodini S. et al., 2009, ApJ, 703, 982

Gnedin N. Y., Hollon N., 2012, ApJS, 202, 13

Gonzalez A. H., Sivanandam S., Zabludoff A. I., Zaritsky D., 2013, ApJ, 778, 14

Grimm H.-J., Gilfanov M., Sunyaev R., 2003, MNRAS, 339, 793

Gunn J. E., Gott, III J. R., 1972, ApJ, 176, 1

Guo Q. et al., 2011, MNRAS, 413, 101

Hopkins P. F., Kereš D., Oñorbe J., Faucher-Giguère C.-A., Quataert E., Murray N., Bullock J. S., 2014, MNRAS, 445, 581

Kang X., van den Bosch F. C., 2008, ApJ, 676, L101

Kannan R., Stinson G. S., Macciò A. V., Brook C., Weinmann S. M., Wadsley J., Couchman H. M. P., 2014a, MNRAS, 437, 3529

Kannan R. et al., 2014b, MNRAS, 437, 2882

Kellogg E., Gursky H., Tananbaum H., Giacconi R., Pounds K., 1972, ApJ, 174, L65

Kravtsov A., Vikhlinin A., Meshscheryakov A., 2014, ArXiv e-prints

Lada C. J., 2006, ApJ, 640, L63

Leitherer C. et al., 1999, ApJS, 123, 3

Lu Z., Mo H. J., Lu Y., 2015, MNRAS, 450, 606

McCarthy I. G., Frenk C. S., Font A. S., Lacey C. G., Bower R. G., Mitchell N. L., Balogh M. L., Theuns T., 2008, MNRAS, 383, 593

Mei S. et al., 2009, ApJ, 690, 42

Mineo S., Gilfanov M., Sunyaev R., 2012, MNRAS, 419, 2095

Narayan R., Medvedev M. V., 2001, ApJ, 562, L129

Navarro J. F., Eke V. R., Frenk C. S., 1996, MNRAS, 283, L72

Navarro J. F., Frenk C. S., White S. D. M., 1995, MNRAS, 275, 56

Navarro J. F., Frenk C. S., White S. D. M., 1997, ApJ, 490, 493

Paczyński B., 1971, ARAA, 9, 183

Peng Y., Maiolino R., Cochrane R., 2015, ArXiv e-prints

Persic M., Rephaeli Y., Braito V., Cappi M., Della Ceca R., Franceschini A., Gruber D. E., 2004, A&A, 419, 849

Pfahl E., Rappaport S., Podsiadlowski P., 2003, ApJ, 597, 1036

Planck Collaboration et al., 2013, A&A, 550, A128

Podsiadlowski P., Rappaport S., Pfahl E. D., 2002, ApJ, 565, 1107

Poggianti B. M., Smail I., Dressler A., Couch W. J., Barger A. J., Butcher H., Ellis R. S., Oemler, Jr. A., 1999, ApJ, 518, 576

Pratt G. W., Croston J. H., Arnaud M., Böhringer H., 2009, A&A, 498, 361

Rees M. J., Ostriker J. P., 1977, MNRAS, 179, 541

Sanderson A. J. R., O'Sullivan E., Ponman T. J., Gonzalez A. H., Sivanandam S., Zabludoff A. I., Zaritsky D., 2013, MNRAS, 429, 3288

Sarazin C. L., 1986, Reviews of Modern Physics, 58, 1

Sato K., Matsushita K., Gastaldello F., 2009, PASJ, 61, 365

Sijacki D., Springel V., Di Matteo T., Hernquist L., 2007, MNRAS, 380, 877

Sijacki D., Springel V., Haehnelt M. G., 2009, MNRAS, 400, 100

Spitzer L., 1962, Physics of Fully Ionized Gases

Springel V., 2010, MNRAS, 401, 791

Springel V., Di Matteo T., Hernquist L., 2005, MNRAS, 361, 776

Springel V., Hernquist L., 2003, MNRAS, 339, 289

Stadel J. G., 2001, PhD thesis, UNIVERSITY OF WASHINGTON

Stinson G., Seth A., Katz N., Wadsley J., Governato F., Quinn T., 2006, MNRAS, 373, 1074

Taylor J. E., Babul A., 2001, ApJ, 559, 716

Verbunt F., van den Heuvel E. P. J., 1995, X-ray Binaries, 457

Vikhlinin A. et al., 2009, ApJ, 692, 1033
Vogelsberger M., Genel S., Sijacki D., Torrey P., Springel V., Hernquist L., 2013, MNRAS, 436, 3031
Voit G. M., 2011, ApJ, 740, 28
Voit G. M., Cavagnolo K. W., Donahue M., Rafferty D. A., McNamara B. R., Nulsen P. E. J., 2008, ApJ, 681, L5
Voit G. M., Donahue M., 2015, ApJ, 799, L1
Voit G. M., Donahue M., Bryan G. L., McDonald M., 2014, ArXiv e-prints
Wadsley J. W., Stadel J., Quinn T., 2004, New Astronomy, 9, 137
Wang L., Li C., Kauffmann G., De Lucia G., 2007, MNRAS, 377, 1419
Wang L. et al., 2014, MNRAS, 439, 611
Weinmann S. M., Kauffmann G., von der Linden A., De Lucia G., 2010, MNRAS, 406, 2249
Weinmann S. M., Lisker T., Guo Q., Meyer H. T., Janz J., 2011, MNRAS, 416, 1197
Weinmann S. M., van den Bosch F. C., Yang X., Mo H. J., 2006, MNRAS, 366, 2
White S. D. M., Rees M. J., 1978, MNRAS, 183, 341
Zakamska N. L., Narayan R., 2003, ApJ, 582, 162